Araya, R. E., Gomez Castro, M. F., Carasi, P., McCarville, J. L., Jury, J., Mowat, A. M., Verdu, E. F. and Chirdo, F. G. (2016) Mechanisms of innate immune activation by gluten peptide p31-43 in mice. American Journal of Physiology: Gastrointestinal and Liver Physiology, 311(1), G40-G49.

There may be differences between this version and the published version. You are advised to consult the publisher's version if you wish to cite from it.

http://eprints.gla.ac.uk/155549/

Deposited on: 31 January 2018

Enlighten – Research publications by members of the University of Glasgow
http://eprints.gla.ac.uk

MECHANISMS OF INNATE IMMUNE ACTIVATION BY GLUTEN PEPTIDE P31-43 IN MICE.

Romina E. Araya[1], María Florencia Gomez Castro[1], Paula Carasi[2], Justin L. McCarville[3], Jennifer Jury[3], Allan M. Mowat[4], Elena F. Verdu[3], Fernando G. Chirdo[1]

[1]Instituto de Estudios Inmunológicos y Fisiopatológicos (IIFP)(CONICET-UNLP). Facultad de Ciencias Exactas. Universidad Nacional de La Plata. La Plata. Argentina.

[2]Catedra de Microbiología. Facultad de Ciencias Exactas. Universidad Nacional de La Plata. La Plata. Argentina.

[3]Farncombe Family Digestive Health Research Institute, McMaster University, Hamilton, Canada.

[4]Centre for Immunobiology, Institute of Infection, Immunity and Inflammation, University of Glasgow, Glasgow G12 8TA, Scotland, UK.

ABSTRACT

Celiac disease (CD) is an immune-mediated enteropathy triggered by gluten in genetically susceptible individuals. Innate immunity contributes to the pathogenesis of CD, but the mechanisms remain poorly understood. Although previous *in vitro* work suggests that gliadin peptide p31-43 acts as an innate immune trigger, the underlying pathways are unclear and have not been explored *in vivo*. Here we show that intraluminal delivery of p31-43 induces morphological changes in the small intestinal mucosa of normal mice consistent with those seen in CD, including increased cell death and expression of inflammatory mediators. The effects of p31-43 were dependent on MyD88 and Type I IFNs, but not TLR4, and were enhanced by co-administration of the TLR3 agonist poly I:C. Together these results indicate that gliadin peptide p31-43 activates the innate immune pathways *in vivo,* such as IFN-dependent inflammation, relevant to CD. Our findings also suggest a common mechanism for the potential interaction between dietary gluten and viral infections in the pathogenesis of CD.

INTRODUCTION

Celiac disease (CD) is a multifactorial disorder triggered by the ingestion of gluten in susceptible individuals who carry the HLA-DQ2 and/or HLA-DQ8 predisposing alleles. Both innate and adaptive immune mechanisms are involved in the pathogenesis of CD. While the adaptive immune response has been well studied, less is known about innate mechanisms and their triggers (1). Some gluten-derived peptides could initiate this process, but there is not enough *in vivo* experimental evidence to confirm this hypothesis. The study of whether and how innate immune mechanisms are induced by gluten peptides is relevant to CD pathophysiology.

Several non-immunogenic gluten peptides that stimulate innate immune responses (termed “toxic peptides”) but not the adaptive immune response have been proposed. Studies have shown that a mix of gluten peptides, pepsin-trypsin digested gliadin (PT-gliadin), activated dendritic cells (26) and peripheral blood mononuclear cells (16) *in vitro*, but identification of the responsible peptides was not achieved. The most studied toxic peptide is the derived α-gliadin p31-43 (LGQQQPFPPQQPY) that is part of the longer peptide p31-55 (LGQQQPFPPQQPYPQPQPFPSQQPY), and is resistant to digestive enzymes in the gut (19). Increased IL-15 production and enterocyte apoptosis were reported in duodenal biopsies of celiac patients incubated with p31-43 (18). p31-43 was also shown to interact with epidermal growth factor receptor (EGFR) (5) and with the IL-15/IL-15R complex (6, 24), to affect proliferative activity in intestinal biopsies, influence human fibroblasts (23), and induce oxidative stress and endosome maturation in enterocytes (17). In murine tissues, p31-43 induced pro-inflammatory cytokines by macrophages (34). Altogether, these studies suggest a role for p31-43 in the stimulation of innate immune mechanisms in CD. However, the underlying pathways and *in vivo* relevance remain unclear.

Type I IFNs are thought to play a role in CD pathogenesis, as there is increased expression of IFNα in duodenal mucosa from CD patients (22) and blockade of IFNα inhibits gliadin-induced IFNγ expression in ex vivo experiments (28). Furthermore epidemiological studies suggest that enteric viral infections such as rotavirus might trigger inflammatory or functional gastrointestinal disease (20, 35). The aim of this study was to determine whether p31-43 elicits innate immune activation in murine small intestine *in vivo* and to investigate potential underlying pathways. We also analyzed the effect of combined intraluminal administration of p31-43 and poly I:C, which mimics a viral infection, a proposed trigger of CD.

MATERIALS AND METHODS

Mice

Eight-week old male C57BL/6J mice were purchased from the Animal Care Facility of the Facultad de Ciencias Exactas y Naturales of the Universidad de Buenos Aires. Eight-week old male MyD88 KO (B6.129P2(SJL)-Myd88tm1.1Defr/J) mice were purchased from the Jackson Laboratory. IFNαR KO mice (IFN-αβR$^{-/-}$, IFNAR$^{-/-}$) on C57BL/6 background were kindly provided by M. Albert (Institute Pasteur, Paris, France). Eight-week old male C3H-HeJ mice were kindly provided by Dr. Martin Rumbo from Instituto de Estudios Inmunológicos y Fisiopatológicos (IIFP-CONICET, Buenos Aires, Argentina). Mice were housed in specific pathogen free condition and fed *ad libitum* with balanced food and autoclaved water. They were maintained on a 12h light/darkness cycle and acclimatized to the surrounding conditions for 1 week before the experimental procedures. All the studies were performed in accordance with international protocols for laboratory animal care (Canadian Council on Animal Care). Experiments were conducted with approval from the Institutional Animal Care and Use Committee of the Facultad de Ciencias Exactas, Universidad Nacional de La Plata.

Intraluminal administration of peptides and poly I:C

p31-43 peptide (LGQQQPFPPQQPY, Biomatik), non-related peptide (NRP) (LDPLIRGLLARPACALQV, Think Peptides), polyinosinic:polycytidylic acid (Sigma Aldrich, poly I:C), a combination of p31-43 peptide and poly I:C, or phosphate buffered saline (PBS) were administered intraluminally during intestinal microsurgery as previously described (3). Briefly, mice were anaesthetized with 80mg/kg ketamine and 10mg/kg xylazine. Once asleep, 100µl of 100µg/ml peptide solution in PBS, 30µg/g poly I:C solution or a combination of p31-43 and poly I:C were injected into the small intestinal lumen, 2cm below the pylorus, to avoid degradation by pancreatic enzymes. Control mice received PBS. After surgery, fluid replacement was administered and mice were monitored until recovery. C57BL/6 mice were sacrificed 2 to 72h post-treatment, while C3H-HeJ, IFNαR KO, and MyD88 KO mice were sacrificed 12h post-treatment.

To compare the effects of p31-43, poly I:C and p31-43+poly I:C in C57BL/6 mice, histological evaluation was performed at 72h post treatment. This time point was chosen based on the previous finding indicating significant differences between treatments at this time.

Histological evaluation

Sections of proximal small intestine of treated mice were fixed in 10% formalin, embedded in paraffin, and stained with H&E for histological evaluation using a Nikon Eclipse Ti fluorescence microscope with X-Cites Series 120 Q light source. Images were taken with Nikon Digital Sight DS Ri1 camera using Nis-Elements software and measurements were performed using Image J software.

Two sections of the proximal small intestine were scored for inflammation in a blinded fashion, with at least thirty villus-to-crypt ratios assessed in each mouse. Intraepithelial lymphocytes (IELs) per 30 enterocytes in ten randomly chosen villus tips were counted according to previously described methods and expressed as IELs/100 enterocytes (7). Histological scores were obtained following the Park-Chiu criteria (27): 0, normal mucosa; 1, subepithelial space at villus tips; 2, extension of subepithelial space with moderate lifting; 3, massive lifting down sides of villi, some denuded tips; 4, denuded villi, dilated capillaries; 5, disintegration of *lamina propria*; 6, Crypt layer injury; 7, transmucosal infarction; 8, transmural infarction.

Real Time PCR

Small Intestinal samples from C57BL/6 mice were stored in RNA Later in -80ºC freezer until use. Tissues were disrupted and RNA extraction was performed using RNeasy Mini Kit (Qiagen). cDNA synthesis was performed from isolated RNA samples (2-5μg), using iScript Reverse Transcription Supermix (Bio-Rad). Real Time PCR was performed with SsoFastEvaGreen Supermix (Bio-Rad) using appropriate forward and reverse primers and the iQ5 thermocycler with fluorescence detection (Bio-Rad). Reactions were run in triplicates. The Real Time PCR (qPCR) protocol was: Cycle 1 (1X) 95°C for 10min; Cycle2 (40X) 60°C for 1min and 95° for 15sec. Primers were synthesized as described previously (9) (**Table 1**) The geometric mean of housekeeping gene HPRT was used as an internal control to normalize the variability in expression levels. All results were expressed as fold increase of each treatment versus the mean of PBS treatment in every time point ($2^{-\Delta\Delta Ct}$ method).

Isolation of epithelial cells and flow cytometric analysis

Sections of proximal small intestine (10 cm) of PBS and p31-43-treated C57BL/6 mice were collected into cold calcium and magnesium free Hanks` Balanced Salt Solution (HBSS, Gibco). Tissue sections were then incubated in HBSS containing 2% v/v fetal bovine serum (FBS, Gibco) and 0.1 mM Dithriothreitol (DTT, Sigma) at 4°C for 10 minutes before being incubated for 15 minutes at 37°C in HBSS with 0.5 mM EDTA (Sigma) with shaking. The cell suspensions were then filtered through an 80μm filter

mesh (BD Biosciences) before use. One million cells were used for flow cytometry analysis and the remaining cells were stored in RNA Later (Ambion) for Real Time PCR analysis of Bax and Bcl2 mRNA expression as described above. For flow cytometric analysis, cells were washed twice with Annexin V Binding Buffer and incubated for 30 minutes at room temperature using Annexin V-FITC (Immunotools). One minute before cell acquisition propidium iodide (5 μg/tube) was added. Cells were analyzed in a BD FACSCalibur flow cytometer (BD Bioscience) and data were processed using CELLQest (BD Bioscience) software.

Confocal microscopy

Small intestinal sections were deparaffinized and treated with Antigen Retrieval AR-10 Solution (BioGenex). After blocking with 2% goat serum, a primary antibody was added for 1h. Anti-Ki67 antibody (Novus Biologicals) was added ON at 4°C and Alexa488 goat anti-rabbit antibody (Molecular Probes) was added at 10μg/ml for 1h. Anti-cleaved caspase-3 antibody conjugated to FITC (Cell Signaling) was added for 1h at RT. Nuclei were stained with propidium iodide at 1μg/ml for 15 minutes. Images were obtained and analyzed in a TCS SP5 Confocal Microscope combined with Leica LAS AF software.

TUNEL reaction

Cell death was quantified using the In Situ Cell Death Detection Kit (Roche). Paraffin-embedded small intestinal tissue sections were dewaxed, rehydrated and treated with Proteinase K for permeabilization. TUNEL reaction mixture was then added and samples were analyzed by confocal microscopy. Images were taken from a confocal microscope Olympus FV1000 (Tokyo, Japan) using a 20x NA 0.75 objective and a zoom of 2x. A 473nm solid-state laser 473 nm was used to detect apoptotic cells while a 405nm state laser was used to identify nuclei stained with DAPI. Images were analyzed with ImageJ software.

Statistical analysis

Statistical analysis was performed with GraphPad Prism software. When two groups were compared, an unpaired t test was used. When more than two groups were compared, a one-way ANOVA test was used; $p<0.05$ was considered significant. Data are displayed as mean ±SEM.

RESULTS

Intraluminal p31-43 peptide induces pathological changes in the murine small intestine.

We used a previously developed technique to deliver molecules of interest intraluminally (3) and tested the capacity of p31-43 to induce morphological changes in small intestinal mucosa. At 12h post p31-43 administration, we observed shortening and widening of villi, increased cell infiltration in the *lamina propria* and edema. Administration of PBS or NRP did not cause intestinal damage (**Figure 1A**). At this time point, we also observed reduction in V/C ratios, increased IEL counts, and higher histological scores in mice treated with p31-43 compared to PBS and NRP (**Figure 1B)**. At 72h, mice treated with p31-43 exhibited persistent edema and cellular infiltration in the LP (**Figure 1A**), reduced V/C ratios, increased number of IELs, and higher histological score compared with PBS and NRP-treated mice (**Figure 1B**). Although the surgical procedure itself altered intestinal histology transiently (3) PBS and NRP-treated mice (controls) experienced faster recovery than p31-43-treated mice (**Figure 1B**). We also evaluated the proliferative activity in small intestinal crypts by counting $Ki67^+$ epithelial cells. At 12h proliferative activity was significantly higher in p31-43 than in PBS-treated mice (**Figure 2A**).

Intraluminal p31-43 increases mRNA expression of inflammatory cytokines.

We next explored the expression of pro-inflammatory mediators induced by p31-43. In comparison with PBS-treated mice, there was a rapid and marked increase in IFNγ mRNA 2h after p31-43 treatment, followed by increases in CXCL10 and IFNβ mRNA, which peaked 6h after intraluminal administration of p31-43 (**Figure 2B**). The expression of mRNA for IL-15, IL-18, IL-1β, IL-6 and TNFα, and chemokines such as MCP1, CXCR3 and CXCL2 was similar in all groups (**data not shown**).

Intraluminal p31-43 induces cell death in the mucosa.

Cell death by gluten specific and non-specific cytotoxic mechanisms plays a role in intestinal damage in CD (31). To study whether p31-43 has cytotoxic activity, we examined TUNEL staining of small intestinal sections 12h after treatment. This revealed a large increase in the number of $TUNEL^+$ cells in the *lamina propria* compared with PBS-treated mice (**Figure 3A**). $TUNEL^+$ cells were also found in the epithelium of p31-43-treated, but not in PBS-treated mice (**white arrows, Figure 3A**). Automated counting confirmed an increase in the frequency of total $TUNEL^+$ cells, when both the *lamina propria* and epithelium of p31-43-treated mice were analyzed (**Figure 3B**). The expression of anti- and pro-apoptotic mediators, Bcl2 and Bax,

respectively, was evaluated by qPCR analysis of whole small intestinal mucosa. At 12h, we found increased Bax/Bcl2 ratio in p31-43-treated mice compared with PBS-treated controls (**Figure 3C**), suggesting that p31-43 has a pro-apoptotic effect in the small intestine *in vivo*. Mice treated with p31-43 had increased numbers of $TUNEL^+$ cells in epithelium compared to PBS-treated control mice (**Figure 3D**). A similar trend was seen in *lamina propria* alone, although this did not attain statistical significance. To further explore the hypothesis that p31-43 caused death of epithelial cells, we first used qPCR analysis of isolated epithelial cells, which showed a trend towards an increase in the Bax/Bcl2 ratio in intraepithelial cells (IEC) from p31-43-treated mice. Although this difference did not reach statistical significance (**Figure 3E**), flow cytometry showed increased number of Annexin V^+/Propidium $Iodide^+$ in IEC from mice treated with p31-43 (**Figure 3F**).

Mucosal changes induced by p31-43 are MyD88- and Type I IFN-, but not TLR4-dependent.

To investigate possible signaling pathways that might mediate the effects of p31-43, we used MyD88 KO, IFNαR KO and TLR4 deficient (C3H-HeJ) mice. No histological changes were observed in MyD88 KO mice 12h after administration of p31-43 (**Figure 4A)**. There were no differences in V/C ratio, IEL counts, global histological scores (**Figure 4B**), or in cell death analysis (**Figure 4C**) between p31-43 and PBS-treated mice. However, TLR4 deficient C3H-HeJ mice had decreased V/C ratios, increased IELs counts and increased global histological scores after administration of p31-43 (**Figure 4D**). The effects of p31-43 were absent in IFNαR KO (**Figure 4E**).

P31-43 and poly I:C cause mucosal damage via independent mechanisms.

Intraluminal administration of poly I:C, a synthetic analogue of dsRNA that mimics the innate response to viral infection acting via TLR3 receptor, induces mucosal damage (3). We therefore investigated the effect of intraluminal administration of p31-43 and poly I:C on mucosal damage. Based on previous work that determined an optimal time point for the induction of intestinal damage and inflammation with poly I:C and reduced effect of surgery at 72 hours (3), we used this time point to evaluate the combined effect of p31-43 and poly I:C. As expected, p31-43 treated mice had reduced V/C ratios compared with control mice at 72h (**Figure 1C and Figure 5A**), but poly I:C alone or the combination of p31-43+poly I:C had a more pronounced decrease in V/C ratios (**Figure 5A**).

P31-43 and poly I:C induce distinct pattern of inflammatory mediators

The analysis of mRNA at different time points after treatment showed distinct patterns of expression for the proinflammatory cytokines IFNβ, IFNγ and TNFα in p31-43, poly I:C or p31-43+poly I:C-treated mice. Increased expression of IFNβ in the mucosa was

found 2h after treatment with poly I:C, whereas this increase was only noted 4h post p31-43+poly I:C treatment. Induction of IFNβ was modest and delayed until 6h after treatment with p31-43 alone. TNFα expression was increased by poly I:C or p31-43+poly I:C, but not by p31-43 treatment. Consistent with previous results, p31-43 induced IFNγ expression, which was not observed in p31-43+poly I:C or poly I:C-treated mice. Poly I:C is a strong inducer of CXCL10 (8), which was also upregulated by p31-43+poly I:C treatment, while CXCL10 induction by p31-43 was weaker and delayed. A synergistic effect of p31-43+poly I:C was only observed for CXCL2 and MCP1 (**Figure 5B**). Altogether, these results suggest that mucosal damage caused by p31-43 and poly I:C may employ different pathways, which can interact in a complex fashion.

Poly I:C enhances cell death induced by p31-43.

Treatment with p31-43 led to increased cell death in the intestinal mucosa as assessed by TUNEL staining (**Figure 3**) and this was further increased in mice given p31-43+poly I:C together. However, poly I:C alone had no effect on cell death (**Figure 6A**). Confirming our previous findings, p31-43 alone also induced a pro-apoptotic pattern of Bax/Bcl2 ratio 12h after treatment, but this was not seen in mice receiving poly I:C alone or in combination with p31-43 (**Figure 6B**). On the other hand, treatment with p31-43+poly I:C induced a marked increase in the number of cleaved-caspase 3 positive cells in *lamina propria* compared with mice treated with PBS, poly I:C or p31-43 alone (**Figure 6C**). As caspase 3 is central to both the intrinsic and extrinsic pathways of apoptosis, these results suggest that p31-43+poly I:C is a stronger stimulus for cell death than poly I:C or p31-43 alone and that the pathways involved may be different.

DISCUSSION

In this study we found that intraluminal administration of p31-43 reduced V/C ratio, increased IEL infiltration and led to higher histological scores in wild type (C57BL/6) mice. P31-43 caused an inflammatory response in the small intestine, characterized by elevation IFNγ expression followed by elevations in IFNβ and CXCL10. P31-43 also induced cell death in epithelial cells. Treatment with p31-43 in mice lacking TLR4 induced similar morphological changes than in wild type, but not in mice lacking the MyD88 molecule. The results indicate a direct pro-inflammatory effect of p31-43 *in vivo,* that requires the central adaptor of the TLR pathway, MyD88, but is independent of TLR4. Finally, we demonstrated that the mucosal damage induced by p31-43 is type I IFN dependent.

There is controversy on the potential induction of the innate immune response by gliadin peptides. Critiques are based on the lack of specific receptor identification and reports on *in vivo* effects. P31-43 has been shown to trigger inflammation using cell lines and duodenal biopsies, while instillation of p31-49 into the duodenum of treated CD patients led to reduced villus/crypt ratios and increased IEL counts within 4h after administration(4, 33). Others have shown that chemokines IP-10 (CXCL10) and MCP-5, which recruit monocytes and T cells, were increased *in vitro* by p31-43 (34), as well as cell proliferation and pro-apoptotic activity (4, 6, 12). In this study, we provide evidence for *in vivo* innate immune stimulation and apoptosis by p31-43. We found that intraluminal p31-43 stimulated a broad spectrum of pro-inflammatory genes such as IFNγ, CXCL10 and IFNβ, increased the number of $Ki67^+$ cells in crypts of C57BL/6 mice, and cellular death in *lamina propria* and in epithelial cells. A high number of $TUNEL^+$ cells were found in p31-43-treated mice, which was associated with a pro-apoptotic profile (high Bax/Bcl2 ratio). Finally, cell death evaluated by qPCR (Bax/Bcl2 ratio), fluorescence microcopy (TUNEL reaction) and flow cytometry (annexin V/ Propidium Iodide) indicated that p31-43 may induce enterocyte death in vivo.

Some previous studies demonstrated that pepsyn-trypsin digested (PT)-gliadin induced pro-inflammatory genes in a MyD88 dependent, but TLR2 and TLR4 independent manner (34), while others showed that gliadin-derived peptides increased inflammatory mediators through TLR4/MyD88/TRIF/MAPK/NFκB and NLRP3 inflammasome pathways (25). Although these findings suggest that innate response via TLR signaling and inflammasome can be elicited by gliadin peptides, p31-43 was not specifically evaluated. Type I IFNs play a critical role in our experimental model, as p31-43 induced the expression of type I IFNs *in vivo* and its effects on intestinal pathology were absent in IFNαR KO mice. Type I IFNs have been suggested as early mediators of CD

pathogenesis and MxA, a downstream element of the Type I IFN pathway, has been reported to be increased in duodenal biopsies of untreated CD patients (13). Although it is not known what factors might drive the induction of Type I IFNs in patients at risk of CD, viral infection is an obvious potential candidate (15, 31, 32). A role for Type I IFNs might also overlap with the proposed involvement of IL-15 in CD (15), as although these mediators activate different downstream pathways, IL-15 upregulation during experimental virus infection depends on IFNαR signaling (11). Our data suggest that p31-43 and viral infection could act in synergy to induce the innate immune responses such as IL-15 production thought to be critical for the initiation of tissue pathology in CD. In order to test whether pathways induced by p31-43 and other stimuli synergize to worsen the innate immune response, we employed a poly I:C model (3). We observed distinct proinflammatory patterns in p31-43, poly I:C, or p31-43+poly I:C-treated mice. Poly I:C alone increased IFNβ, TNFα and CXCL10. p31-43 alone induced IFNβ and CXCL10 at lower levels, and it was the only stimuli that rapidly increased IFNγ. The combination of p31-43 and poly I:C increased IFNβ, TNFα, CXCL10, and was the only stimuli that increased CXCL2 and MCP-1. CXCL10, CXCL2 and MCP-1 are relevant for the recruitment of T cells, polymorphonuclear cells and monocytes.

Analysis by TUNEL staining, Bax/Bcl2 ratio and cleaved caspase 3, suggests that a pro-apoptotic pathway is involved in the increased cell death observed in p31-43-treated mice. In contrast, poly I:C treatment did not induce a significant increase in any of these parameters, perhaps indicating that the histological damage caused by these stimuli may be driven by different pathways. As well as cell apoptosis, mechanisms such as metalloproteases- and TGFβ-induced fibrosis can all contribute to tissue pathology and these may be induced differentially by individual triggers. Further support for complexity in the pathogenic processes could come from our finding that in p31-43+poly I:C-treated mice, the number of $TUNEL^+$ cells and of cleaved caspase 3^+ cells was increased, but there was no change in Bax/Bcl2 ratio. Since caspase 3 can be activated by both intrinsic and extrinsic apoptotic pathways, but also can be cleaved by Granzyme B (10), this may explain why in p31-43+poly I:C treated mice cleaved caspase 3 and $TUNEL^+$ cells were increased but not the pro-apoptotic ratio. Together our results suggest that distinct or partially overlapping pathways of tissue damage may be induced by p31-43 and poly I:C.

The adaptive immune response in CD is necessary for the development of the disease, however it is now clear that it is insufficient to cause full intestinal pathology (21). Cytotoxic activity of IELs has been considered as a key element for enterocyte damage. Though increased number and activation of IELs are a hallmark of CD, how these cells are induced and activated is still a matter of discussion. Setty et al. have recently suggested that epithelial stress and anti-gluten adaptive immune responses

can be independently induced at early stages of the disease (30). In accordance with these results, previous reports from our group revealed the presence of epithelial stress in active CD (2). Altogether, the results raise the hypothesis that by activating innate immunity, peptides such as p31-43 may lead to epithelial stress, a condition that together with the adaptive immune response would facilitate the development of enteropathy in CD. . It remains to be determined whether this mechanisms could also have implications for other gluten-related disorders such as non-celiac gluten sensitivity (29). Our work shows that induction of inflammation by non-immunogenic peptides depends on MyD88, but not TLR4, signaling. In contrast, wheat amylase-trypsin inhibitors (ATIs), have been identified as potent stimulators of an inflammatory reaction through activation of TLR4 signaling on monocytes, macrophages and dendritic cells (14). Therefore, it is possible that non-immunogenic gluten peptides and non-gluten proteins in wheat induce inflammation through different pathways facilitating the onset of CD and other intestinal inflammatory diseases.

In summary, *in vivo* inflammatory changes driven by p31-43 and poly I:C occur through different pathways, as judged by the kinetics of the mucosal damage and histological recovery. Though the receptor for p31-43 has not been identified yet, different cells can produce inflammatory mediators after incubation with this peptide. Since HLA-DQ2 or DQ8 molecules do not present p31-43 and the mucosal changes observed are MyD88- and Type I IFN- dependent, future work should determine the effect of p31-43 in other genetically modified mouse strains. Signals triggered by gliadin-derived peptides, particularly p31-43, in addition to those elicited by certain infections, may exacerbate inflammation promoting the development of intestinal pathology in a genetically susceptible individual.

ACKNOWLEDGEMENTS

This work was supported by Grants to F.Ch. from CONICET PIP 719 and PICT 2012 1030. E.F.V. is funded by a CIHR grant MOP-142773. R.E.A. is a CONICET Scholar. J.L.M. is a Boris Family Scholar.

REFERENCES

1. **Abadie V**, **Jabri B**. IL-15: A central regulator of celiac disease immunopathology. *Immunol Rev* 260: 221–234, 2014.

2. **Allegretti YL**, **Bondar C**, **Guzman L**, **Cueto Rua E**, **Chopita N**, **Fuertes M**, **Zwirner NW**, **Chirdo FG**. Broad MICA/B Expression in the Small Bowel Mucosa: A Link between Cellular Stress and Celiac Disease. *PLoS One* 8: e73658, 2013.

3. **Araya RE**, **Jury J**, **Bondar C**, **Verdu EF**, **Chirdo FG**. Intraluminal Administration of Poly I:C Causes an Enteropathy That Is Exacerbated by Administration of Oral Dietary Antigen. *PLoS One* 9: e99236, 2014.

4. **Barone M**, **Troncone R**, **Auricchio S**. Gliadin Peptides as Triggers of the Proliferative and Stress/Innate Immune Response of the Celiac Small Intestinal Mucosa. *Int J Mol Sci* 15: 20518–20537, 2014.

5. **Barone M V**, **Gimigliano A**, **Castoria G**, **Paolella G**, **Maurano F**, **Paparo F**, **Maglio M**, **Mineo A**, **Miele E**, **Nanayakkara M**, **Troncone R**, **Auricchio S**. Growth factor-like activity of gliadin, an alimentary protein: implications for coeliac disease. *Gut* 56: 480–488, 2007.

6. **Barone MV**, **Zanzi D**, **Maglio M**, **Nanayakkara M**, **Santagata S**, **Lania G**, **Miele E**, **Ribecco MTS**, **Maurano F**, **Auricchio R**, **Gianfrani C**, **Ferrini S**, **Troncone R**, **Auricchio S**. Gliadin-mediated proliferation and innate immune activation in celiac disease are due to alterations in vesicular trafficking. *PLoS One* 6: e17039, 2011.

7. **Biagi F**, **Luinetti O**, **Campanella J**, **Klersy C**, **Zambelli C**, **Villanacci V**, **Lanzini A**, **Corazza GR**. Intraepithelial lymphocytes in the villous tip: do they indicate potential coeliac disease? *J Clin Pathol* 57: 835–839, 2004.

8. **Bratland E**, **Hellesen A**, **Husebye ES**. Induction of CXCL10 chemokine in adrenocortical cells by stimulation through toll-like receptor 3. *Mol Cell Endocrinol* 365: 75–83, 2013.

9. **Bustin S a**, **Benes V**, **Garson J a**, **Hellemans J**, **Huggett J**, **Kubista M**, **Mueller R**, **Nolan T**, **Pfaffl MW**, **Shipley GL**, **Vandesompele J**, **Wittwer CT**. The MIQE guidelines: minimum information for publication of quantitative real-time PCR experiments. *Clin Chem* 55: 611–22, 2009.

10. **Clarke P**, **Tyler KL**. Apoptosis in animal models of virus-induced disease. *Nat Rev Microbiol* 7: 144–55, 2009.

11. **Colpitts SL**, **Stoklasek TA**, **Plumlee CR**, **Obar JJ**, **Guo C**, **Lefrançois L**. Cutting edge: the role of IFN-α receptor and MyD88 signaling in induction of IL-15 expression in vivo. *J Immunol* 188: 2483–7, 2012.

12. **D'Arienzo R**, **Stefanile R**, **Maurano F**, **Luongo D**, **Bergamo P**, **Mazzarella G**, **Troncone R**, **Auricchio S**, **David C**, **Rossi M**. A deregulated immune response to gliadin causes a decreased villus height in DQ8 transgenic mice. *Eur J Immunol* 39: 3552–61, 2009.

13. **Iacomino G**, **Marano A**, **Stillitano I**, **Aufiero VR**, **Iaquinto G**, **Schettino M**, **Masucci A**, **Troncone R**, **Auricchio S**, **Mazzarella G**. Celiac disease: role of intestinal compartments in the mucosal immune response. *Mol Cell Biochem* 411: 341–9, 2016.

14. **Junker Y**, **Zeissig S**, **Kim S-J**, **Barisani D**, **Wieser H**, **Leffler DA**, **Zevallos V**, **Libermann TA**, **Dillon S**, **Freitag TL**, **Kelly CP**, **Schuppan D**. Wheat amylase

trypsin inhibitors drive intestinal inflammation via activation of toll-like receptor 4. *J Exp Med* 209: 2395–408, 2012.

15. **Kim SM**, **Mayassi T**, **Jabri B**. Innate immunity: actuating the gears of celiac disease pathogenesis. *Best Pract Res Clin Gastroenterol* 29: 425–35, 2015.

16. **Lammers KM**, **Khandelwal S**, **Chaudhry F**, **Kryszak D**, **Puppa EL**, **Casolaro V**, **Fasano A**. Identification of a novel immunomodulatory gliadin peptide that causes interleukin-8 release in a chemokine receptor CXCR3-dependent manner only in patients with coeliac disease. *Immunology* 132: 432–440, 2011.

17. **Luciani A**, **Villella VR**, **Vasaturo A**, **Giardino I**, **Pettoello-Mantovani M**, **Guido S**, **Cexus ON**, **Peake N**, **Londei M**, **Quaratino S**, **Maiuri L**. Lysosomal accumulation of gliadin p31–43 peptide induces oxidative stress and tissue transglutaminase-mediated PPARγ downregulation in intestinal epithelial cells and coeliac mucosa. *Gut* 59: 311–319, 2010.

18. **Maiuri L**, **Ciacci C**, **Ricciardelli I**, **Vacca L**, **Raia V**, **Auricchio S**, **Picard J**, **Osman M**, **Quaratino S**, **Londei M**. Association between innate response to gliadin and activation of pathogenic T cells in coeliac disease. *Lancet* 362: 30–7, 2003.

19. **Mamone G**, **Ferranti P**, **Rossi M**, **Roepstorff P**, **Fierro O**, **Malorni A**, **Addeo F**. Identification of a peptide from α-gliadin resistant to digestive enzymes: Implications for celiac disease. *J Chromatogr B Anal Technol Biomed Life Sci* 855: 236–241, 2007.

20. **Marshall JK**, **Thabane M**, **Borgaonkar MR**, **James C**. Postinfectious Irritable Bowel Syndrome After a Food-Borne Outbreak of Acute Gastroenteritis Attributed to a Viral Pathogen. *Clin Gastroenterol Hepatol* 5: 457–460, 2007.

21. **Meresse B**, **Malamut G**, **Cerf-Bensussan N**. Celiac Disease: An Immunological Jigsaw. *Immunity* 36: 907–919, 2012.

22. **Monteleone G**, **Pender SL**, **Alstead E**, **Hauer AC**, **Lionetti P**, **McKenzie C**, **MacDonald TT**. Role of interferon alpha in promoting T helper cell type 1 responses in the small intestine in coeliac disease. [Online]. *Gut* 48: 425–9, 2001. http://www.pubmedcentral.nih.gov/articlerender.fcgi?artid=1760133&tool=pmcentrez&rendertype=abstract [18 Apr. 2016].

23. **Nanayakkara M**, **Kosova R**, **Lania G**, **Sarno M**, **Gaito A**, **Galatola M**, **Greco L**, **Cuomo M**, **Troncone R**, **Auricchio S**, **Auricchio R**, **Barone MV**. A celiac cellular phenotype, with altered LPP sub-cellular distribution, is inducible in controls by the toxic gliadin peptide P31-43. *PLoS One* 8: e79763, 2013.

24. **Nanayakkara M**, **Lania G**, **Maglio M**, **Discepolo V**, **Sarno M**, **Gaito A**, **Troncone R**, **Auricchio S**, **Auricchio R**, **Barone MV**. An undigested gliadin peptide activates innate immunity and proliferative signaling in enterocytes: the role in celiac disease. *Am J Clin Nutr* 98: 1123–1135, 2013.

25. **Palová-Jelínková L**, **Dáňová K**, **Drašarová H**, **Dvořák M**, **Funda DP**, **Fundová P**, **Kotrbová-Kozak A**, **Černá M**, **Kamanová J**, **Martin SF**, **Freudenberg M**, **Tučková L**. Pepsin Digest of Wheat Gliadin Fraction Increases Production of IL-1β via TLR4/MyD88/TRIF/MAPK/NF-κB Signaling Pathway and an NLRP3 Inflammasome Activation. *PLoS One* 8: e62426, 2013.

26. **Palová-Jelínková L**, **Rozková D**, **Pecharová B**, **Bártová J**, **Sedivá A**, **Tlaskalová-Hogenová H**, **Spísek R**, **Tucková L**. Gliadin fragments induce phenotypic and functional maturation of human dendritic cells. [Online]. *J Immunol* 175: 7038–45, 2005. http://www.ncbi.nlm.nih.gov/pubmed/16272365 [4 Oct. 2015].

27. **Quaedackers JSLT**, **Beuk RJ**, **Bennet L**, **Charlton A**, **oude Egbrink MGA**, **Gunn AJ**, **Heineman E**. An evaluation of methods for grading histologic injury following ischemia/reperfusion of the small bowel. *Transplant Proc* 32: 1307–1310, 2000.

28. **Di Sabatino A**, **Pickard KM**, **Gordon JN**, **Salvati V**, **Mazzarella G**, **Beattie RM**, **Vossenkaemper A**, **Rovedatti L**, **Leakey NAB**, **Croft NM**, **Troncone R**, **Corazza GR**, **Stagg AJ**, **Monteleone G**, **MacDonald T**. Evidence for the Role of Interferon-alfa Production by Dendritic Cells in the Th1 Response in Celiac Disease. *Gastroenterology* 133: 1175–1187, 2007.

29. **Sapone A**, **Lammers KM**, **Casolaro V**, **Cammarota M**, **Giuliano MT**, **De Rosa M**, **Stefanile R**, **Mazzarella G**, **Tolone C**, **Russo MI**, **Esposito P**, **Ferraraccio F**, **Cartenì M**, **Riegler G**, **de Magistris L**, **Fasano A**. Divergence of gut permeability and mucosal immune gene expression in two gluten-associated conditions: celiac disease and gluten sensitivity. *BMC Med* 9: 23, 2011.

30. **Setty M**, **Discepolo V**, **Abadie V**, **Kamhawi S**, **Mayassi T**, **Kent A**, **Ciszewski C**, **Maglio M**, **Kistner E**, **Bhagat G**, **Semrad C**, **Kupfer SS**, **Green PH**, **Guandalini S**, **Troncone R**, **Murray JA**, **Turner JR**, **Jabri B**. Distinct and Synergistic Contributions of Epithelial Stress and Adaptive Immunity to Functions of Intraepithelial Killer Cells and Active Celiac Disease. *Gastroenterology* 149: 681–691.e10, 2015.

31. **Sollid LM**, **Jabri B**. Triggers and drivers of autoimmunity: lessons from coeliac disease [Online]. *Nat Rev Immunol* 13: 294–302, 2013. http://dx.doi.org/10.1038/nri3407.

32. **Stene LC**, **Honeyman MC**, **Hoffenberg EJ**, **Haas JE**, **Sokol RJ**, **Emery L**, **Taki I**, **Norris JM**, **Erlich HA**, **Eisenbarth GS**, **Rewers M**. Rotavirus Infection Frequency and Risk of Celiac Disease Autoimmunity in Early Childhood: A Longitudinal Study [Online]. *Am J Gastroenterol* 101: 2333–2340, 2006. http://dx.doi.org/10.1111/j.1572-0241.2006.00741.x.

33. **Sturgess R**, **Day P**, **Ellis HJ**, **Lundin KE a**, **Gjertsen H a.**, **Kontakou M**, **Ciclitira PJ**. Wheat peptide challenge in coeliac disease. *Lancet* 343: 758–761, 1994.

34. **Thomas KE**, **Sapone A**, **Fasano A**, **Vogel SN**. Gliadin stimulation of murine macrophage inflammatory gene expression and intestinal permeability are MyD88-dependent: role of the innate immune response in Celiac disease. *J Immunol* 176: 2512–2521, 2006.

35. **Verdu EF**, **Mauro M**, **Bourgeois J**, **Armstrong D**. Clinical onset of celiac disease after an episode of Campylobacter jejuni enteritis. *Canada J Gastroenterol* 21: 453–455, 2007.

TABLE 1: PRIMERS USED FOR QUANTITATIVE PCR

Gene	Forward	Reverse
HPRT	CAATGCAAACTTTGCTTTCC	CAAATCCAACAAAGTCTGGC
IFNβ	AATGGAAAGATCAACCTCAC	AAGGCAGTGTAACTCTTCTG
CXCL10	ATAGGGAAGCTTGAAATCATCC	TTCATCGTGGCAATGATCTC
CXCR3	TGTAGTTGGGCTAGCTCGAACTT	ACCTGGATATATGCTGAGCTGTCA
TNFα	CTCCCTCTCATCAGTTCTATGG	TTGAGAAGATGATCTGAGTGTG
IL-15	CATCCATCTCGTGCTACTTGTGTT	CATCTATCCAGTTGGCCTCTGTTT
MCP1	CTACAAGAGGATCACCAGCAG	TTCTGATCTCATTTGGTTCCG
CXCL2	AAGATACTGAACAAAGGCAAGG	TTCTTTCTCTTTGGTTCTTCCG
IL-1β	CGTTCCCATTAGACAACTGC	CTCATGGAGAATATCACTTGTTGG
IL-18	GATCAAAGTGCCAGTGAACC	GATCTTGTTCTTACAGGAGAGG
IL-6	CATGTTCTCTGGGAAATCGT	TATATCCAGTTTGGTAGCATCC
IFNγ	CTGAGACAATGAACGCTACAC	TTTCTTCCACATCTATGCCAC
Bax	TGCTACAGGGTTTCATCCAG	ATTGCTGTCCAGTTCATCTC
Bcl2	GATCTCTGGTTGGGATTCCT	ACAACTTGCAATGAATCGGG

LEGENDS TO FIGURES

Figure 1: Intraluminal p31-43 peptide induces pathological changes in the murine small intestine.

Representative H&E stained sections of proximal small intestine of C57BL/6 mice after 12h and 72h of intraluminal administration of p31-43, NRP or PBS. Black scale bar: 100μm. Red arrows show edema and Light Blue arrows show some IELs (A). Morphological analysis of small intestine from C57BL/6 mice: villus-to-crypt (V/C) ratio, number of IELs and histological score after 12h (B) and 72h (C) (Stats: N= 4 mice per group, Unpaired t test, *P<0.05, **P<0.01, ***P<0.001).

Figure 2: Intraluminal p31-43 peptide produces hyperproliferation in crypts and a proinflammatory response in small intestine.

Evaluation of the proliferative activity in small intestinal crypts by $Ki67^+$ cell counts. After 12h post-treatment with p31-43 or PBS, samples of small intestine were stained with anti-Ki67 antibody. Images were obtained and analyzed in a TCS SP5 Confocal Microscope. The plots show the number of $Ki67^+$ cells per crypt. (Stats: N= 4 mice per group, Unpaired t test, **P<0.01) (A). Real Time-PCR analysis of small intestinal samples from C57BL/6 mice after intraluminal administration of p31-43 or PBS was performed. Plots show mRNA expression after 2 to 12h of p31-43 (black dots) or PBS (empty dots) treatment. IFNγ, IFNβ, and CXCL10 mRNA expression was assessed. All values were normalized with the housekeeping mRNA expression (HPRT). Results were expressed as fold increase of every treatment versus the mean of PBS treatment in every time point ($2^{-\Delta\Delta Ct}$ method). (Stats: N= 4 mice per group, Unpaired t test, *P<0.05, **P<0.01, p31-43-treated mice versus PBS control in the same time point).

Figure 3: Intraluminal p31-43 induces cell death in the small intestinal mucosa.

Sections of small intestine after 12h post-treatment with p31-43 or PBS were stained with TUNEL reaction. Sections were analyzed by confocal microscopy. Images were taken from a confocal microscope Olympus FV1000. White arrows point some $TUNEL^+$ nuclei in the epithelial layer. White scale bar: 100μm (A). $TUNEL^+$/total cells from mucosa were determined using ImageJ software (B). The expression of anti- and pro-apoptotic mediators, Bcl2 and Bax, respectively, was evaluated by quantitative PCR analysis of small intestinal mucosa; results were plotted as Bax/Bcl2 ratio (C). $TUNEL^+$/total cells from epithelium and *lamina propria*, separately, were determined using ImageJ software (D). Epithelial cells were isolated from small intestine 12h after treatment with p31-43 or PBS and the expression of Bcl2 and Bax was evaluated by quantitative PCR; results were plotted as Bax/Bcl2 ratio (E). Isolated epithelial cells

were stained with Annexin V and Propidium Iodide and analyzed by flow cytometry (F). (Stat: N= 4 mice per group, Unpaired t test, *P<0.05, **P<0.01, p31-43-treated mice versus PBS control)

Figure 4: Changes induced by p31-43 are MyD88- and type I IFN-dependent.

Representative H&E stained sections of proximal small intestine of MyD88 mice after 12h and 72h of intraluminal administration of p31-43 or PBS. Black scale bar: 100µm (A). Morphological analysis of small intestine from MyD88 KO mice treated with p31-43 or PBS: villus-to-crypt (V/C) ratio, number of IELs and histological score after 12h (B). Small intestinal sections after 12h post-treatment with p31-43 or PBS were stained with TUNEL reaction. Sections were analyzed by confocal microscopy. Images were taken from a confocal microscope Olympus FV1000. White scale bar: 100µm. $TUNEL^{+}$/total cells from mucosa were determined using ImageJ software (C). Morphological analysis of small intestine from C3H/HeJ mice (TLR4 deficient mice) treated with p31-43 or PBS: Villus-to-crypt (V/C) ratio, number of IELs and histological score after 12h (D). Morphological analysis of small intestine from $IFN\alpha R^{-/-}$ mice treated with p31-43 or PBS: villus-to-crypt (V/C) ratio, number of IELs and histological score, after 12h. (Stats: N= 4 mice per group, Unpaired t test, **P<0.01, ***P<0.001).

Figure 5: P31-43 and poly I:C cause mucosal damage via independent mechanisms.

Morphological analysis of small intestine from C57BL/6 mice after p31-43, poly I:C (PIC), p31-43+poly I:C or PBS treatment. villus-to-crypt (V/C) ratio was determined after 72h. (Stats: N= 4 mice per group, Unpaired t test, *P<0.05, **P<0.01, all treatment versus PBS control in the same time point) (A). Real Time-PCR analysis of small intestinal samples from C57BL/6 mice after p31-43, poly I:C (PIC), p31-43+poly I:C or PBS administration. Plots show mRNA expression after 2 to 12h of p31-43, poly I:C, p31-43+poly I:C or PBS treatment. IFNγ, IFNβ, TNFα, CXCL10, CXCL2, and MCP1 mRNA expression was assessed. All values were normalized with the housekeeping mRNA expression (HPRT). Results were expressed as fold increase of every treatment versus the mean of PBS treatment in every time point ($2^{-\Delta\Delta Ct}$ method) (Stats: N= 4 mice per group, One-way ANOVA, *P<0.05, **P<0.01, ***P<0.001, every treatment versus PBS control in the same time point)

Figure 6: Poly I:C enhances cell death induced by p31-43.

Sections of small intestine after 12h post-treatment with p31-43 or PBS were stained with TUNEL reaction. Sections were analyzed by confocal microscopy. Images were taken from a confocal microscope Olympus FV1000. White scale bar: 100µm. $TUNEL^{+}$/

567 total cell ratio was determined using ImageJ software (A). The expression of anti- and
568 pro-apoptotic mediators, Bcl2 and Bax, respectively, was evaluated by quantitative
569 PCR analysis of small intestinal mucosa; results were plotted as Bax/Bcl2 ratio (Stat:
570 N= 4 mice per group, Unpaired t test, **P<0.01, p31-43-treated mice versus PBS
571 control) (B). Expression of cleaved caspase 3 was assessed by confocal microscopy.
572 Anti-cleaved caspase 3 antibody conjugated to FITC was used. Nuclei were stained
573 with propidium iodide. Images were obtained and analyzed in a TCS SP5 Confocal
574 Microscope combined with Leica LAS AF software. White scale bar: 100μm (C).

Figure 1

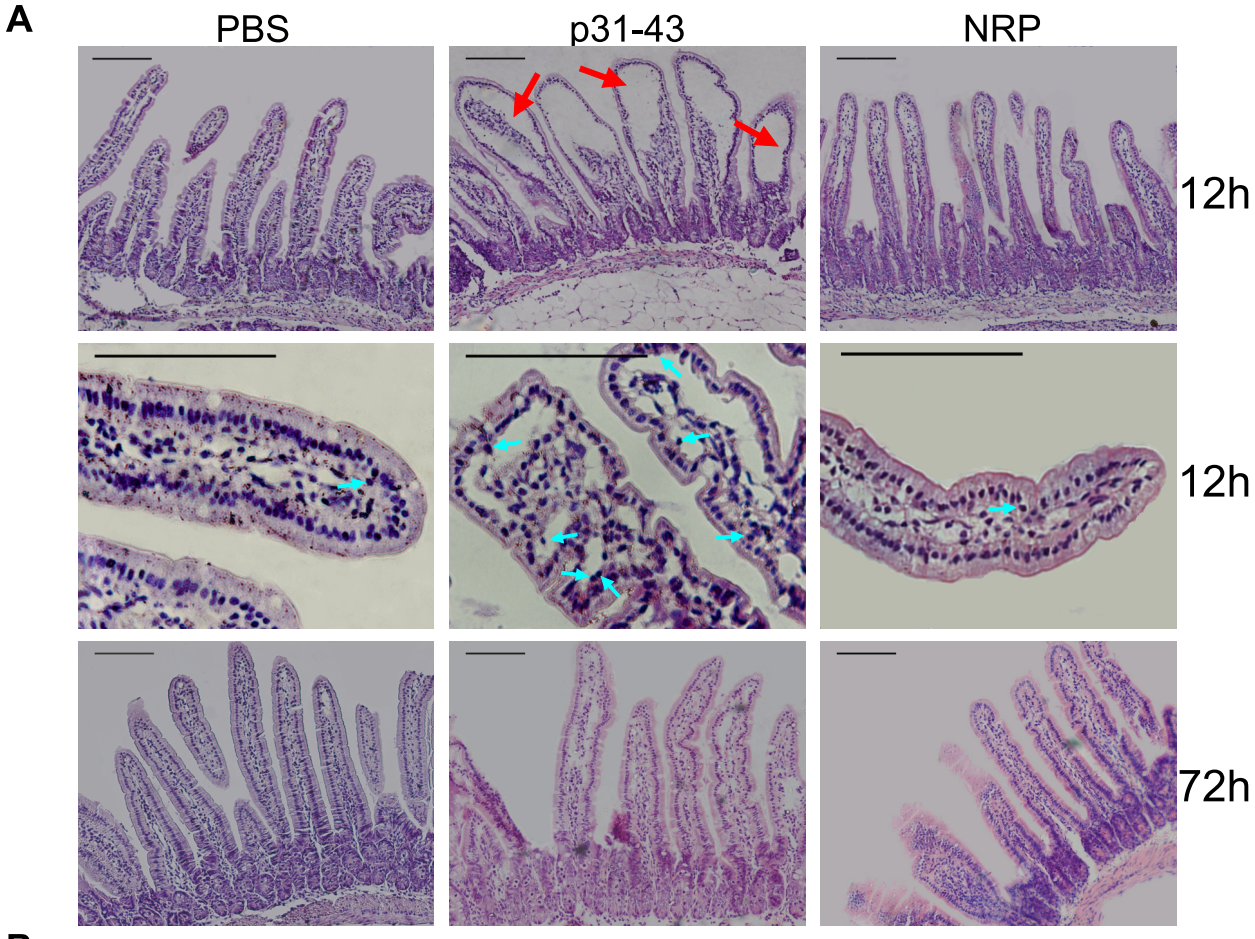
A
PBS
p31-43
NRP
12h
12h
72h
B
V/C ratio
IELs/100 Enterocytes
Histological Score
PBS
p31-43
NRP
C
V/C ratio
IELs/100 Enterocytes
Histological Score
PBS
p31-43
NRP

Figure 2

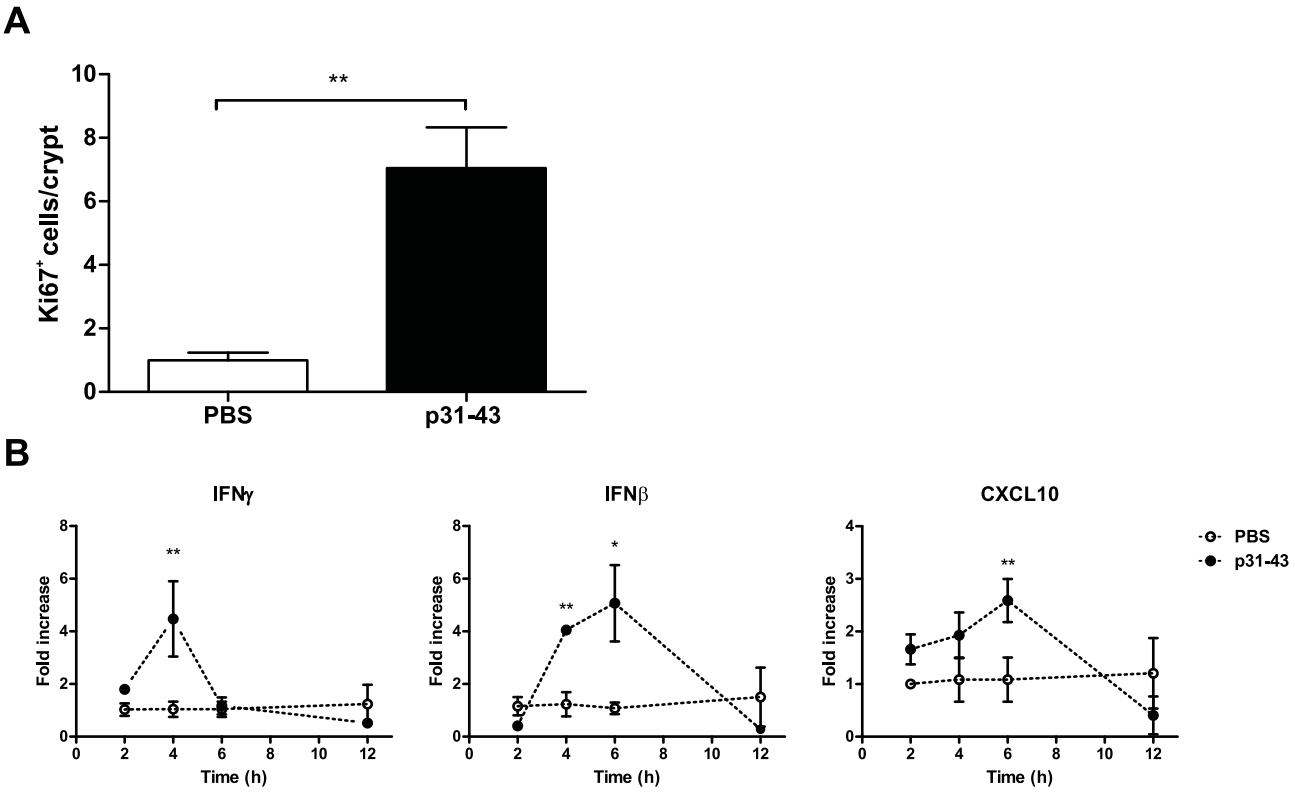
A
Ki67+ cells/crypt
10
8
6
4
2
0
**
PBS
p31-43
B
IFNγ
IFNβ
CXCL10
Fold increase
Time (h)
PBS
p31-43
*
**

Figure 3

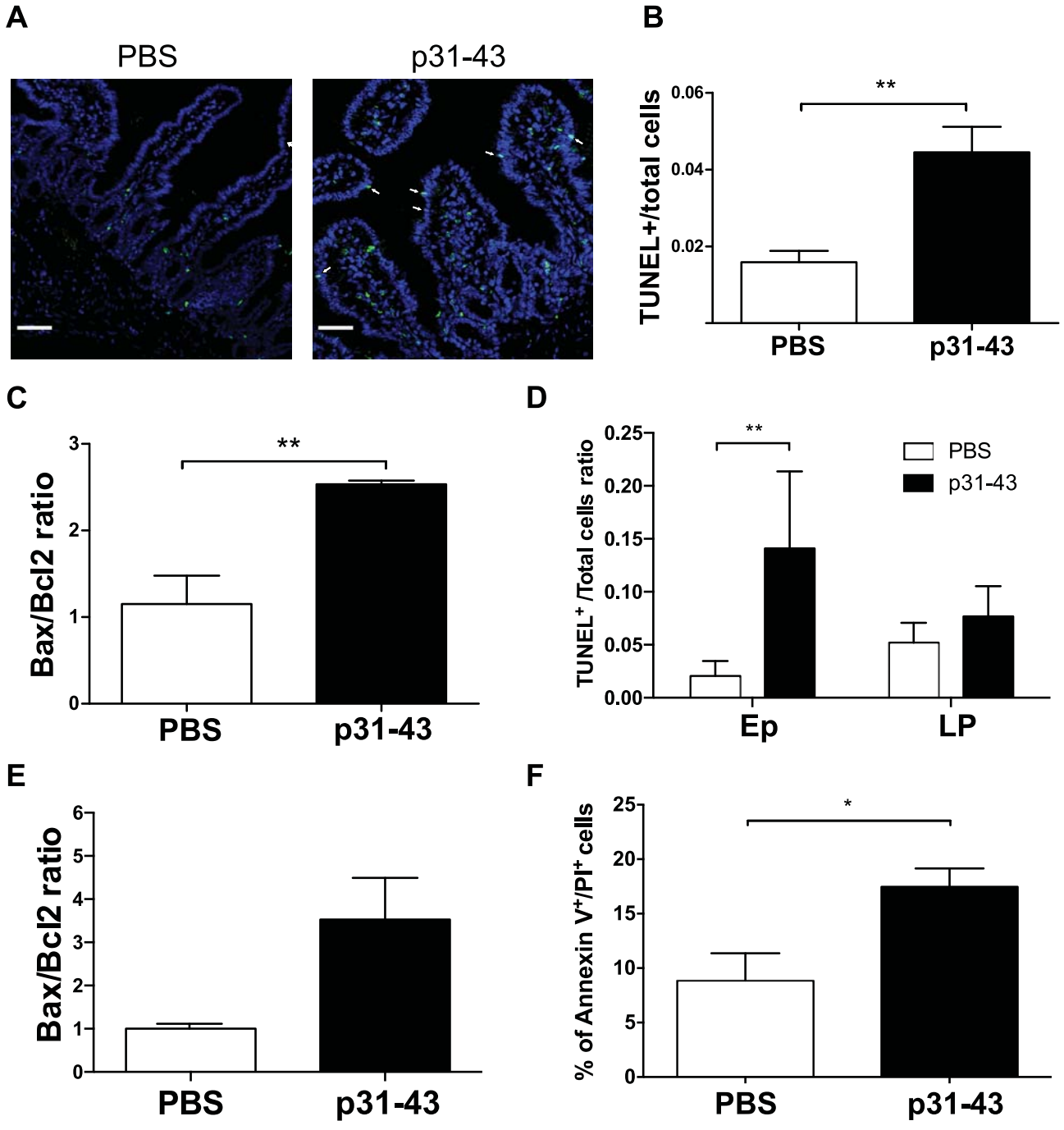
A
PBS
p31-43
B
TUNEL+/total cells
0.06
0.04
0.02
**
PBS
p31-43
C
Bax/Bcl2 ratio
3
2
1
0
**
PBS
p31-43
D
TUNEL+ /Total cells ratio
0.25
0.20
0.15
0.10
0.05
0.00
**
PBS
p31-43
Ep
LP
E
Bax/Bcl2 ratio
6
5
4
3
2
1
0
PBS
p31-43
F
% of Annexin V+/PI+ cells
25
20
15
10
5
0
*
PBS
p31-43

Figure 4

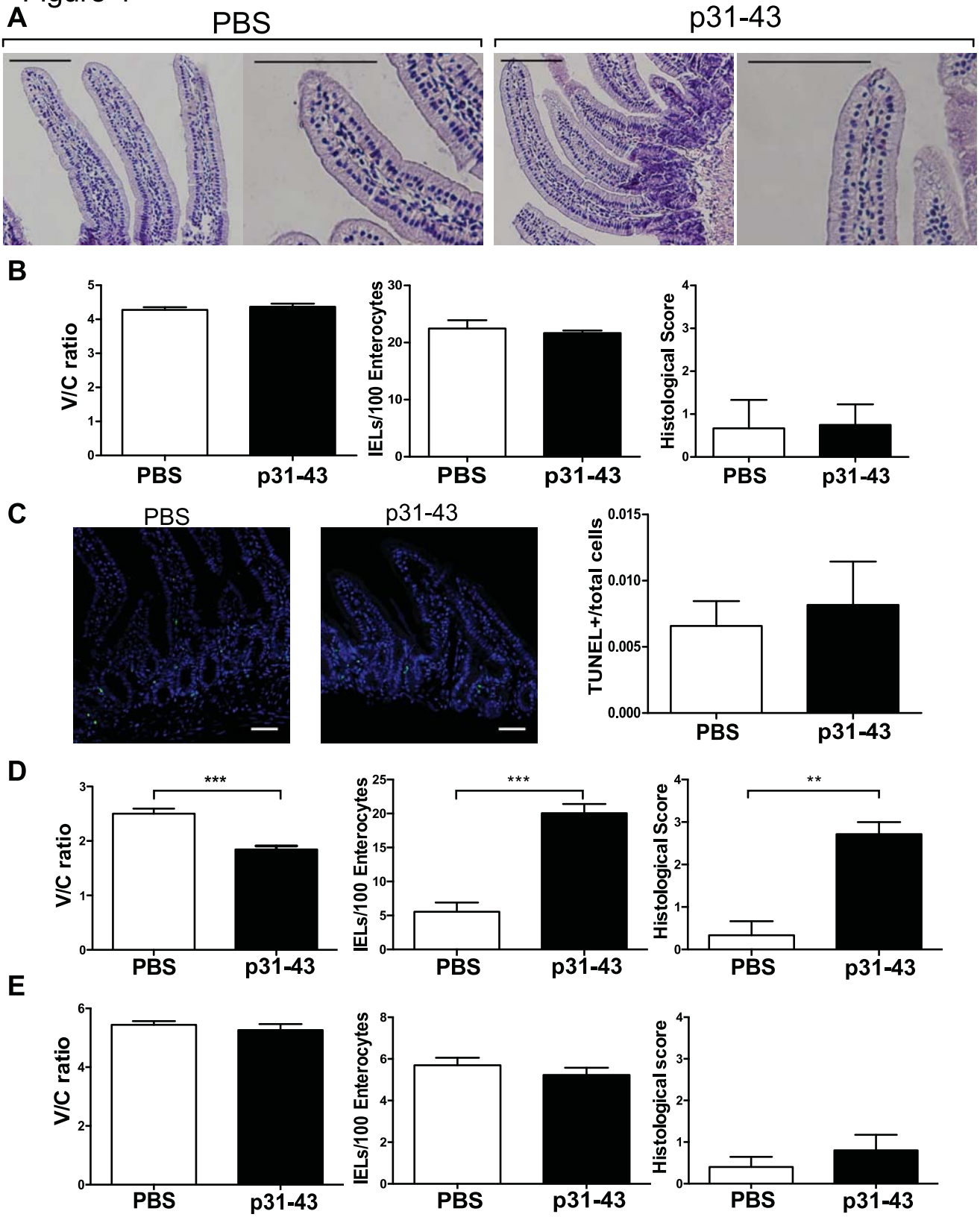
A
PBS
p31-43
B
V/C ratio
IELs/100 Enterocytes
Histological Score
PBS
p31-43
C
PBS
p31-43
TUNEL+/total cells
D
***
***
**
E
Histological score

Figure 5

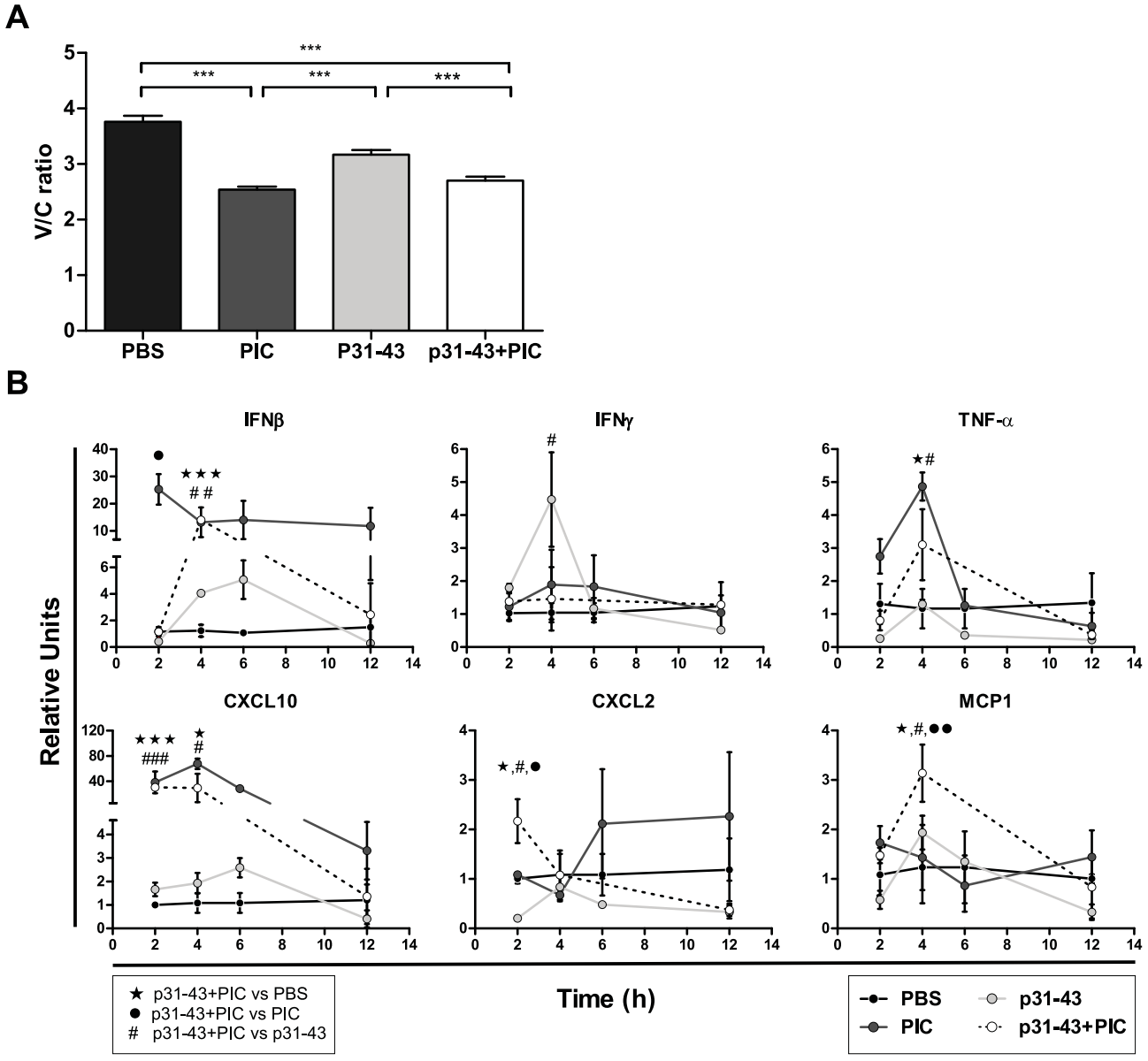
A
***
***
***
***
V/C ratio
PBS
PIC
P31-43
p31-43+PIC
B
IFNβ
IFNγ
TNF-α
CXCL10
CXCL2
MCP1
Relative Units
★ p31-43+PIC vs PBS
● p31-43+PIC vs PIC
p31-43+PIC vs p31-43
Time (h)
PBS
PIC
p31-43
p31-43+PIC

Figure 6

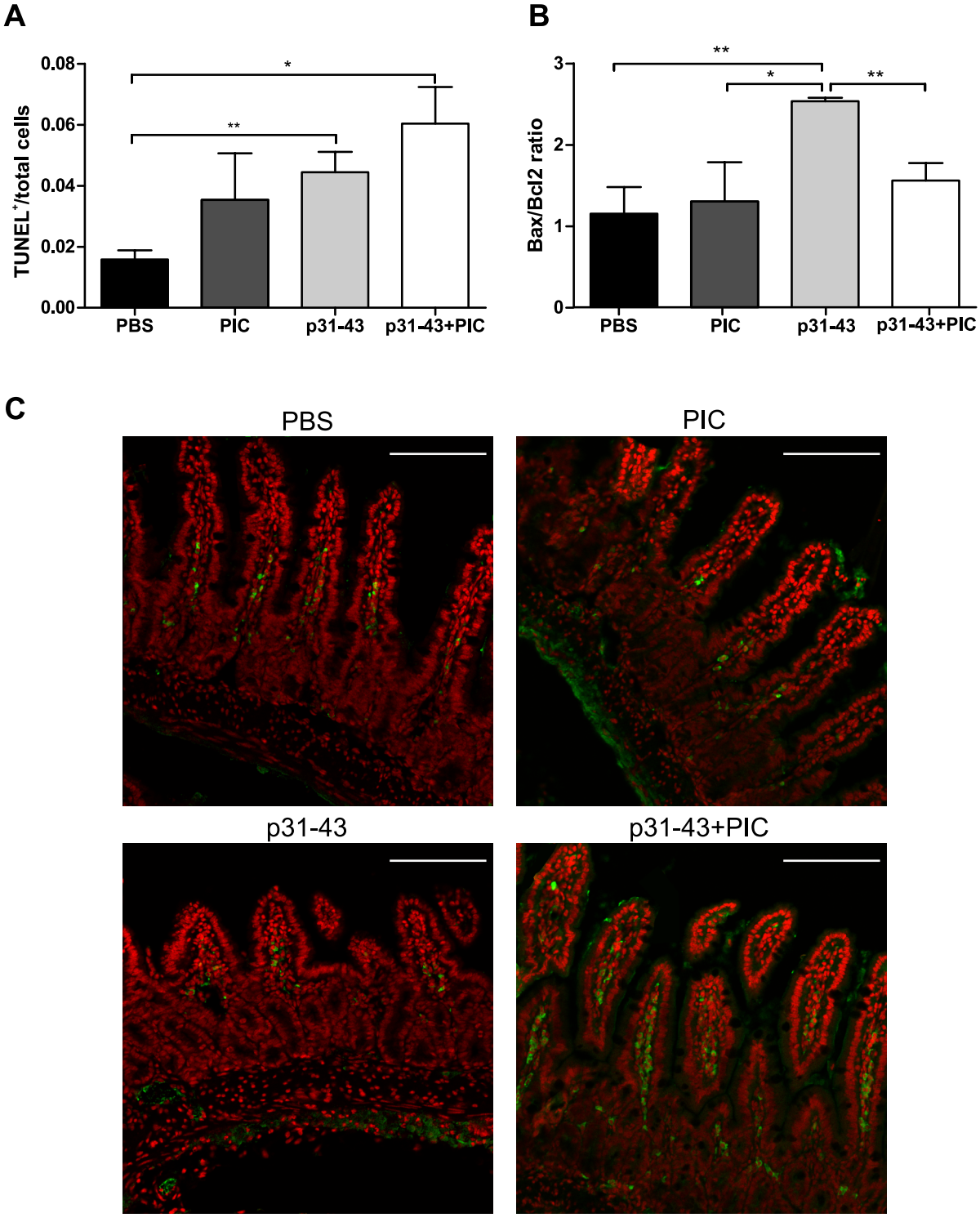
A
TUNEL+/total cells
0.08
0.06
0.04
0.02
0.00
*
**
PBS
PIC
p31-43
p31-43+PIC
B
Bax/Bcl2 ratio
3
2
1
0
**
*
**
PBS
PIC
p31-43
p31-43+PIC
C
PBS
PIC
p31-43
p31-43+PIC